

Development of very small-diameter, inductively coupled magnetized plasma device

D. Kuwahara, A. Mishio, T. Nakagawa, and S. Shinohara

Citation: *Rev. Sci. Instrum.* **84**, 103502 (2013); doi: 10.1063/1.4823524

View online: <http://dx.doi.org/10.1063/1.4823524>

View Table of Contents: <http://rsi.aip.org/resource/1/RSINAK/v84/i10>

Published by the [AIP Publishing LLC](#).

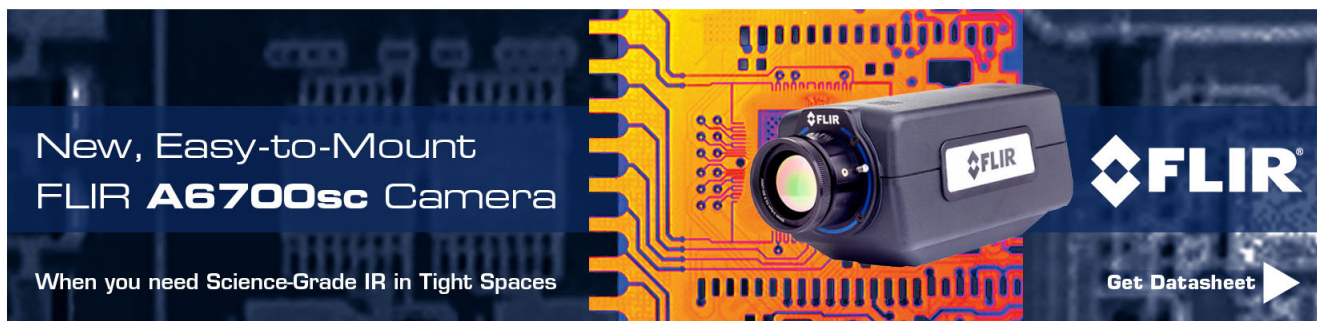
Additional information on *Rev. Sci. Instrum.*

Journal Homepage: <http://rsi.aip.org>

Journal Information: http://rsi.aip.org/about/about_the_journal

Top downloads: http://rsi.aip.org/features/most_downloaded


Information for Authors: <http://rsi.aip.org/authors>



New, Easy-to-Mount
FLIR A6700sc Camera

When you need Science-Grade IR in Tight Spaces

FLIR

Get Datasheet 

The advertisement features a black FLIR A6700sc camera mounted on a yellow and orange printed circuit board. The background is a dark blue grid pattern. The FLIR logo is visible on the camera and in the bottom right corner.

Development of very small-diameter, inductively coupled magnetized plasma device

D. Kuwahara,^{a)} A. Mishio, T. Nakagawa, and S. Shinohara
 Tokyo University of Agriculture and Technology, 2-24-16 Naka-cho, Koganei,
 Tokyo 184-8588, Japan

(Received 21 July 2013; accepted 13 September 2013; published online 2 October 2013)

In order to miniaturize a high-density, inductively coupled magnetized plasma or helicon plasma to be applied to, e.g., an industrial application and an electric propulsion field, small helicon device has been developed. The specifications of this device along with the experimental results are described. We have succeeded in generating high-density ($\sim 10^{19} \text{ m}^{-3}$) plasmas using quartz tubes with very small diameters of 10 and 20 mm, with a radio frequency power ~ 1200 and 700 W , respectively, in the presence of the magnetic field less than 1 kG . © 2013 AIP Publishing LLC. [<http://dx.doi.org/10.1063/1.4823524>]

I. INTRODUCTION

High-density ($\sim 10^{19} \text{ m}^{-3}$), high-ionization ratio (up to several tens of percent) helicon plasmas or inductively coupled magnetized plasma can be produced with wide operating ranges of, e.g., the magnetic field and its strength, a fill pressure, and an excitation radio frequency (rf).¹⁻⁴ Thus, they are utilized in various fields such as a plasma processing and an electric propulsion field, in addition to basic and nuclear fusion ones. Typical, present operating ranges of these are as follows: electron density: 10^{18} – 10^{20} m^{-3} , magnetic field strength:^{5,6} 5×10^{-3} – 1.5 T , rf frequency: 5 – 30 MHz , plasma volume:⁷⁻⁹ 23 cm^3 – 2.1 m^3 , plasma diameter:⁸⁻¹⁰ 20 – 750 mm (including Inductively Coupled Plasma (ICP) (20 mm in diameter)¹¹). Needless to say, it is crucial to expand external operating parameters including plasma sizes.

An application of high-density plasma source to an electric thruster, which has a higher specific impulse than a chemical thruster, a helicon high-density plasma is very useful. For example, in order to solve a problem of an electrode erosion, high-density helicon sources with some acceleration schemes are promising in an electrodeless propulsion system.¹² Since the electrodes have no direct contact with plasmas in this system, it is expected to have a longer operation life time. In addition, the electric thruster using the small-diameter plasma source, developed in this study, will contribute to a light weight thruster such as an attitude controller. Moreover, a clustered-compact thruster enables more redundancy than a single thruster which has the same thrust. According to past studies, the smallest diameter of the helicon electric thruster was 20 mm .^{8,10} Furthermore, the small source is also important to an industrial application such as a coating of inner wall of a thin tube.

However, in constructing a small diameter plasma, there are several problems, e.g., increased ratios of rf sheath and a Larmor radius (ions and electrons) to plasma radius, and enhanced plasma-wall interactions (physical view point). There are also difficulties to measure plasma parameters by various probes inserted into small discharge tubes, and to control and

measure a neutral pressure in the small tube, along with a problem of a coupling between an rf antenna and a plasma (technical view point). Here, this study aims to demonstrate the smallest-diameter (10 and 20 mm), high-density helicon plasma source developed, and to characterize its plasma leading to clarify the above problems in future.

II. DESCRIPTION OF SMALL HELICON DEVICE (SHD)

In order to demonstrate a very small-diameter, high-density helicon plasma, Small Helicon Device (SHD) has been designed and developed. A schematic view of SHD is shown in Fig. 1. This device has 10 and 20 mm in inner diameter (i.d.) discharge tubes, and 5 mm and less i.d. can be applied to check the helicon performance in future from the present design.

A. Vacuum system

Vacuum system of SHD consists of 4 parts, i.e., a gas feeding part, a discharge tube, a vacuum chamber made of SUS316, and a gas pumping part. The gas feeding part is connected to a head flange (leftmost in Fig. 1). An argon gas is supplied through a mass flow controller (SEC-400MK3, HORIBA: mass flow rate of 1 – 30 sccm). The discharge tube made of a quartz (10 or 20 mm i.d. with an axial length of 453 mm) can be connected to a vacuum chamber. In addition, the head flange has a ionization vacuum gauge (MG-2, Canon ANELVA) to measure a neutral gas pressure in a wide range between 10^{-6} and 13 Pa . The vacuum chamber, 165 mm in i.d. and 865 mm in an axial direction, works as a buffer tank of the discharge tube. The vacuum chamber has many flanges, i.e., ten 2.5 in. flanges and four gauge port flanges (as shown in Fig. 1), to accept various diagnostics easily, e.g., Langmuir probes, a fiber of monochromator, and a high-speed camera. A turbo-molecular pump (TG200, 200 l/s , Osaka Vacuum, Ltd.) and a rotary pump (CVD-050A, 50 l/min , ULVAC) are also connected to the vacuum chamber. An ionization gauge is also added near the turbo-molecular pump. The base pressure in

^{a)}Electronic mail: dkuwahar@cc.tuac.ac.jp

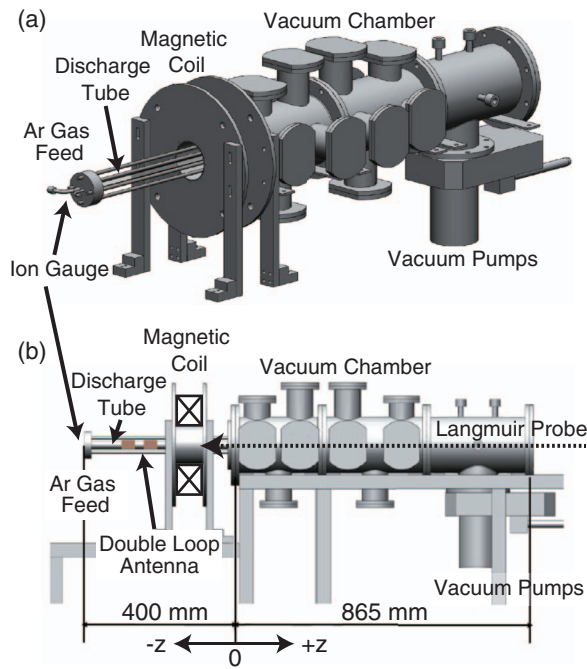


FIG. 1. Schematic of SHD: (a) bird eye view and (b) side view.

the vacuum chamber is less than 10^{-4} Pa, and operating pressure in the source region is between 0.1 and 10 Pa.

B. rf system

The rf system consists of 3 parts: a double-loop antenna for plasma production, an impedance matching circuit, and a rf power supply. This double-loop antenna, made of copper plates of 0.3 mm thickness, is wound around the outer surface of the quartz tube. Two copper plates of 50 mm and 40 mm in width are used with central axial distances of 50 mm and 60 mm, in the case of 10 mm and 20 mm i.d., respectively. In the matching box (T020-6326AK, THAMWAY), a split tank circuit (serial capacitance: 100–35 000 pF, parallel capacitance: 85–5500 pF, series inductance: 1–60 μ H) is employed. In order to estimate an rf-plasma coupling, the rf current and voltage are measured in addition to the incident and reflected powers by a directional coupler with an attenuation of 50 dB. A connection length between the matching box and the double loop antenna is kept as short as possible, using parallel feeder lines made of copper plates. The rf power supply is composed of a function generator (SG4105, IWATSU) and a power amplifier (T145-6326CK, THAMWAY), feeding rf power up to 2 kW with an rf frequency of 0.3–13.56 MHz. Due to heat damages to the antenna and Langmuir probes, the experiment has been carried out in a 100 ms rf discharge pulse with a 1.0 s interval (duty ratio is 1/10).

C. Magnetic field coil

To excite the helicon wave, an external magnetic field is necessary. SHD has a magnetic field coil (404 turns, 90 mm i.d.) in the discharge tube section. Figure 2(a) shows

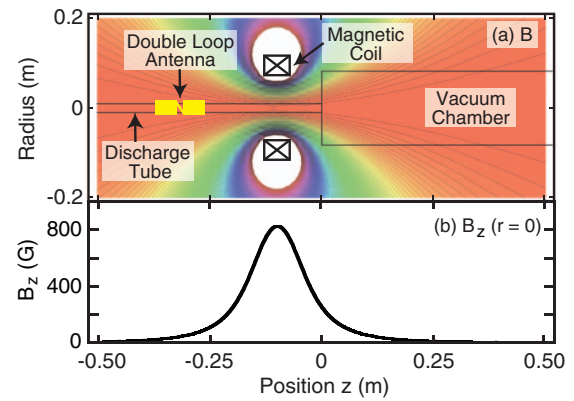


FIG. 2. Schematic diagram of SHD and the profile of the magnetic field. (a) 2D profile of the absolute magnetic field distribution (axial component) and magnetic field lines. (b) Axial (z) distribution of the z component of the magnetic field ($r = 0$), with the coil current of 30 A.

distributions of the magnetic field. The axial magnetic fields B in the center of the magnetic coils are measured as 275, 550, and 825 G with the coil current of 10, 20, and 30 A, respectively, which are in good agreement with calculation results. In the application of the electric propulsion, a divergent magnetic field can produce a thrust with combined effects of $-\mu\nabla B$ and $-\nabla p$ (where μ and p are a magnetic moment and a plasma pressure, respectively), like a role of a magnetic nozzle. Moreover, the divergent field configuration is useful in the electromagnetically plasma acceleration scheme proposed by our group. Since this divergent magnetic field has a radial component B_r , a Lorentz force (thrust) is expected if the azimuthal current j_θ is induced in the plasma by some ways, e.g., rotating magnetic field method^{8,13} and rotating electric field one.^{7,12}

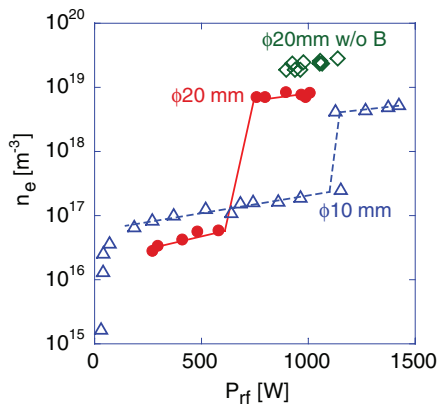
D. Diagnostics

To characterize the plasma performance, electron density profiles were measured by a Langmuir probe, which is inserted from an opposite side of the discharge tube (see Fig. 1). The electron density n_e was derived from the ion saturation current under an assumption of the typical electron temperature T_e of 3 eV. In the case of the small diameter discharge tube, e.g., less than 10 mm i.d., the probe measurement disturbs plasma production very much, since the probe occupies large area in an inner space of the discharge tube. Therefore, spectroscopic measurements using monochromators (MC-150N, Ritu Oyo Kougaku Co., Ltd., wavelength resolution of 0.006 nm, and HR2000+, Ocean Optics, wavelength resolution of 0.5 nm) were used as non-invasive measurements: Doppler shifts and broadenings of emission lines from the plasma in addition to line intensities.

III. EXPERIMENTAL RESULTS

A. Dependence of the electron density on rf power

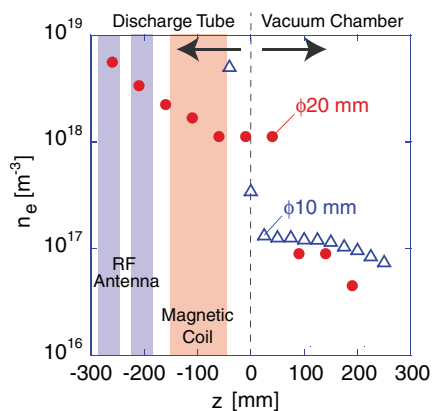
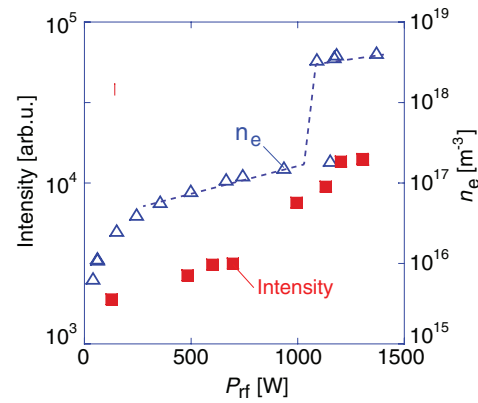
Figure 3 shows n_e obtained in the rf antenna region as a function of the rf power (P_{rf} , incident power – reflected one) with an rf frequency of 7 MHz throughout the present

FIG. 3. n_e responses as a function of P_{rf} .

paper. The experimental conditions are as follows: Langmuir probe position: $z = -265$ mm (center of the excitation antenna), mass flow rate: 5 sccm (~ 2.4 Pa at the head flange position for 10 mm i.d.) and 20 sccm (~ 2.0 Pa for 20 mm i.d.), and magnetic coil current: 20 A. In this figure, electron density jumps were observed at ~ 1200 W (10 mm i.d.) and $P_{rf} \sim 700$ W (20 mm i.d.). Here, in both cases, at the density jumps, n_e increased to be close to 10^{19} m^{-3} by a factor of more than several tens of times. Since n_e was sufficiently high after the jumps, this mode change is considered as a mode change from ICP to helicon plasma. Note that in the 10 mm i.d. case, the low density ($\sim 10^{15}$ m^{-3}) plasma could be generated with very low rf power of several W.

B. Electron density distribution in the axial direction

Figure 4 shows n_e distribution along the axial direction with 10 and 20 mm i.d. tubes under the same experimental conditions as those in Fig. 3 except for $P_{rf} \sim 690$ W. Using 20 mm i.d. tube, n_e decreased with increasing distance from the rf antenna, and it decreased rapidly when a plasma entered the vacuum vessel region from discharge tube where n_e is $> 10^{18}$ m^{-3} . A similar trend of the sudden density drop could be seen in the case of 10 mm i.d. tube, although only one point in the discharge tube was measured: 10 mm i.d.

FIG. 4. n_e distribution in the axial direction.FIG. 5. Ar I emission and n_e as functions of P_{rf} .

case indicates the higher n_e than that in 20 mm i.d. case in the tube region.

C. ICP discharge

Figure 3 also shows the dependence of n_e on P_{rf} without the magnetic field (ICP mode) in the case of i.d. 20 mm (open diamonds). Comparatively high-density plasma more than 10^{19} m^{-3} was generated in the localized region (near the antenna) with $P_{rf} \sim 1$ kW. However, plasma was not produced stably with $P_{rf} < 800$ W.

D. Ar I emission

As a preliminary test of non-invasive diagnostics for the case of very small i.d. tubes, we tried a spectroscopic measurement using a monochromator (HR2000+). Figure 5 shows the dependences of n_e (same experimental conditions as Fig. 3: ϕ 10 mm case) and Ar I intensity on P_{rf} . The intensity of Ar I was obtained at the position of $z = -250$ mm (center of the double-loop antenna). Here, the intensity of Ar I is written as

$$I_{ArI} \propto n_e n_0 \sigma, \quad (1)$$

where I_{ArI} , n_0 , and σ indicate an intensity of Ar I, neutral particle density, and a cross-section depending on T_e , respectively. From Fig. 5, I_{ArI} showed a slight jump at the density jump with $P_{rf} \sim 800$ W. This small jump might come from the decrease (increase) in n_0 (n_e), if we could neglect a change of the σ term.

IV. DISCUSSION

Here, two points are discussed. First point is a particle production efficiency. The total electron number (N_e) in the whole plasma region divided by P_{rf} is considered.^{12,14} In the case of 20 mm i.d., by taking the average n_e in the discharge tube of 2.5×10^{18} m^{-3} , axial plasma length of 400 mm, and P_{rf} of 690 W (see Fig. 4), N_e/P_{rf} is estimated to be $\sim 5 \times 10^{12}$ W^{-1} . This value, which is expected to be proportional to a^2 (a : plasma radius) in the present conditions, is in good agreement with other helicon data^{12,14} and also with the power balance consideration.¹⁴ If the main loss is across

the field, hence efficiency deterioration with a reduction of plasma radius is considered to be the enhanced radial diffusion and the wall loss. Although a helicon plasma was not verified due to non-measurement of wave propagation, this shows an excellent particle production efficiency even in the very small diameter.

Second, a normalized size relating to the plasma-wall interactions is briefly discussed. Since the ion Larmor radius in the condition of Fig. 3 case is calculated to be 6.4 mm (B in the coil center and argon ion temperature are taken of 550 G and 0.3 eV, respectively). When a plasma is away from the magnetic field coil, the diameter of an ion orbit becomes larger than i.d. of discharge tube due to the divergent field. Although there are plasma losses by collisions at the inner wall surface of the discharge tube, we could still keep the high-density plasma (see 20 mm i.d. case in Fig. 4). Needless to say, more experimental data are required in future, i.e., detailed spatial distributions of n_e and a plasma potential, along with wave structures by non-disturbed measurements.

V. CONCLUSION

In this study, in order to investigate the characteristics of the small-diameter helicon plasma, we have developed SHD: A high-density helicon plasma of n_e up to 10^{19} m^{-3} was successfully produced with the smallest i.d. of 10 and 20 mm, by measuring the P_{rf} dependence and an axial distribution.

These results can open a window to a downsized scaling and several problems raised in the Introduction part. In order to have a further reduction of plasma radius, we need to consider technical problems, considering physical one mentioned in the Introduction part, including helicon wave

characteristics such as wave structure and a dispersion relation. It is also necessary to install non-contact diagnostics such as spectroscopy, microwave interferometer, and laser induced fluorescence measurements, since the Langmuir probe disturbs the plasma behavior strongly.

ACKNOWLEDGMENTS

We appreciate useful discussions made by Helicon Electroless Advanced Thruster (HEAT) project members. This research has been partially supported by Grants-in-Aid for Scientific Research (S: 21226019) from the Japan Society for the Promotion of Science.

¹R. W. Boswell, *Phys. Lett. A* **33**, 457 (1970).

²S. Shinohara, *Jpn. J. Appl. Phys.* **36**, 4695 (1997).

³R. W. Boswell and F. F. Chen, *IEEE Trans. Plasma Sci.* **25**, 1229 (1997).

⁴F. F. Chen and R. W. Boswell, *IEEE Trans. Plasma Sci.* **25**, 1245 (1997).

⁵F. R. Chang-Díaz, *Sci. Am.* **283**, 90 (2000).

⁶S. Shinohara, *Jpn. J. Appl. Phys.* **35**, 4503 (1996).

⁷K. Toki, S. Shinohara, T. Tanikawa, I. Funaki, and K. P. Shamrai, in *Proceedings of the 28th International Electric Propulsion Conference, IEPC03-0168* (CNES, Paris, 2003).

⁸S. Shinohara, H. Nishida, T. Tanikawa, T. Hada, I. Funaki, K. P. Shamrai, *Trans. Fusion Sci. Technol.* **63**, 164 (2013).

⁹S. Shinohara and T. Tanikawa, *Rev. Sci. Instrum.* **75**, 1941 (2004).

¹⁰O. V. Batishchev, *IEEE Trans. Plasma Sci.* **37**, 1563 (2009).

¹¹C. S. Corr, J. Zanger, R. W. Boswell, and C. Charles, *Appl. Phys. Lett.* **91**, 241501 (2007).

¹²S. Shinohara, T. Hada, T. Motomura, K. Tanaka, T. Tanikawa, K. Toki, Y. Tanaka, and K. P. Shamrai, *Phys. Plasmas* **16**, 057104 (2009).

¹³I. R. Jones, *Phys. Plasmas* **6**, 1950 (1999).

¹⁴T. Tanikawa and S. Shinohara, in *Proceedings of the International Congress on Plasma Physics* (Association EURATOM-CAE, Cadarache, 2004), see <http://hal.archives-ouvertes.fr/hal-00002013/>.